

High potential performance of Cerium-doped $\text{LiNi}_{0.5}\text{Co}_{0.2}\text{Mn}_{0.3}\text{O}_2$ cathode material for Li-ion battery

Li Xia · Kehui Qiu · Yuyan Gao · Xia He · Fangdong Zhou

Received: 25 September 2014 / Accepted: 13 January 2015 / Published online: 24 January 2015
© Springer Science+Business Media New York 2015

Abstract To enhance the electrochemistry performance of $\text{LiNi}_{0.5}\text{Co}_{0.2}\text{Mn}_{0.3}\text{O}_2$ (NCM-523) cathode material, especially at high rate and high potential charge–discharge, Cerium has been used to dope into the material. Cerium-doped NCM-523 exhibits significantly better rate capability and excellent cycling stability than the pristine material both at conventional potential of 4.25 V and high potential of 4.5 V. Electrochemical tests show that Cerium-doped NCM-523 discharged a 2.56 times higher capacity than pristine sample at 5 C when charged to 4.5 V, versus 1.94 times at 4.25 V. Pristine NCM-523 exhibits the capacity retention of 93.28 and 90.90 % at 1 C after 30 cycles for 4.25 and 4.5 V, respectively. After doping with Cerium, the capacity retention is increased to 96.77 and 97.35 % after cycles. XRD results show that Cerium is successfully doped into $\text{LiNi}_{0.5}\text{Co}_{0.2}\text{Mn}_{0.3}\text{O}_2$ crystal lattice. Such enhanced performance of material should be ascribed to Cerium doping, which stabilizes the layered crystal structure, reduces the dissolution degree of cation in the electrode and improves the lithium-ion diffusion of the oxide proved by the EIS tests.

Introduction

Rechargeable lithium-ion batteries are widely employed for electronic gadgetry with high capacity and long cycle life [1–6]. Recently, most interest has focused on a new system of $\text{LiNi}_{1-x-y}\text{Co}_x\text{Mn}_y\text{O}_2$ ($0 < x < 1$, $0 < y < 1$) with a-NaFeO₂ structure as cathode materials, which have been considered promising to displace LiCoO_2 [7–10]. Among them, $\text{LiNi}_{0.5}\text{Co}_{0.2}\text{Mn}_{0.3}\text{O}_2$ (NCM-523) has attracted much attention because of its excellent initial discharge capacity [11–13]. However, it has a bad rate capability and obvious capacity degradation at high potential cycle, which indeed limits its extensively practical application [14].

To date, many researches have been done to overcome above problems. One way is to cover the cathode materials with various protective layers. The coating layers can reduce the contact area for electrode in electrolyte [15–18]. The other one is to improve the electrochemical performances with doping to modify the structure of cathode materials. The doping of electrode with alkaline earth metal (Mg, Sr) [19, 20], transition metal (V) [21, 22], main group metal (Al) [20], and halogen element (F) [23] have been explored to improve the property of NCM-523. However, there are hardly any reports about the effects of rare earth element on Li-ion battery.

Among all rare earth elements, Cerium has been much widely used in many fields as addition and catalyst. Wu cong [24] has reported that Cerium doping is effective to improve the electrochemical performance of LiFePO_4 . Zhong shengkui [25] has successfully synthesized $\text{LiNi}_{1/3-x}\text{Mn}_{1/3}\text{Co}_{1/3}\text{Ce}_x\text{O}_2$ by a co-precipitation method and proved that Ce-doped $\text{LiNi}_{1/3}\text{Co}_{1/3}\text{Mn}_{1/3}\text{O}_2$ has much better cycling performance and rate capability. In this work, we explore the influence of Cerium doping on the

L. Xia · X. He · F. Zhou
College of Materials and Chemistry and Chemical Engineering,
Chengdu University of Technology, Chengdu 610059, China

K. Qiu (✉)
Institute of Materials Science and Technology, Chengdu
University of Technology, Chengdu 610059, China
e-mail: qkh2188@163.com

Y. Gao
Chengdu Jingyuan New Materials Technology Co., Ltd.,
Chengdu 610100, China

electrochemical performance of NCM-523 at 4.25 V and a higher potential of 4.5 V. The composition, structure, and morphology of the materials were characterized. The impact of Cerium doping on the electrochemical properties, rate capability, cycle ability, and electrochemical impedance spectroscopy was also investigated.

Experimental

$\text{Ni}_{0.5}\text{Co}_{0.2}\text{Mn}_{0.3}(\text{OH})_2$ precursor was firstly achieved by coprecipitation method. $\text{NiSO}_4 \cdot 6\text{H}_2\text{O}$, $\text{CoSO}_4 \cdot 7\text{H}_2\text{O}$, and $\text{MnSO}_4 \cdot \text{H}_2\text{O}$ were dissolved in distilled water (cationic ratio of Ni:Co:Mn = 5:2:3) to obtain a mixed solution with a concentration of 2.0 mol/L. The prepared solution was dripped into the base solution (pH = 11) in nitrogen atmosphere with continuous rapid stirring. In the meantime, 0.5 mol/L $\text{NH}_3 \cdot \text{H}_2\text{O}$ solution as complexant and 2.0 mol/L NaOH solution as precipitant were added separately. The reaction was conducted for 10 h at 60 °C with pH value of 11. The suspension was washed and filtered repeatedly and dried at 100 °C, then $\text{Ni}_{0.5}\text{Co}_{0.2}\text{Mn}_{0.3}(\text{OH})_2$ precursor was obtained.

The layered Cerium-doped NCM-523 materials were synthesized by solid-state method. Precursor was well mixed with Li_2CO_3 and CeO_2 , and sintered at 900 °C in atmosphere for 10 h followed by a nature cooling procedure to achieve layered Cerium-doped NCM-523 cathode materials.

The powder X-ray diffraction (XRD, Dmax-C) with $\text{CuK}\alpha$ radiation was chosen to examine the crystalline phase of the prepared powders. The data were collected over 10–80° (2θ) with a scan rate of 5° per minute.

The particle size and morphology of the synthesized materials were analyzed by a scanning electron microscope (SEM, Hitachi, S-4800).

The electrochemical properties were characterized via CR2032 coin-type cell. The mixed slurry of active material, carbon black, and polyvinylidene fluoride (PVDF) binder with a weight ratio of 94.4:2.5:3.1 in *N*-pyrrolidone (NMP) solvent was prepared and pasted onto an Aluminum current collector. After drying at 90 °C for 2 h, the electrode was rolled and cut. Coin cell was composed of positive electrode, negative electrode (lithium foil), separator (a porous polypropylene film), and electrolyte (1 mol/L LiPF_6 in EC:EMC:DMC (1:1:1 in volume)). Argon-filled glove box (UN800S, Dellix) was employed to assemble coin cells. Initial charge–discharge capacities, rate capability, and cycling performance are measured by Neware battery test system (CT-3008 W, Shenzhen, China) in the potential region of 3–4.25 V and 3–4.50 V at room temperature.

Electrochemical impedance spectroscopy (EIS, CHI660D) tests were performed by an electrochemical

work station, within 5 mV voltage amplitude between 10 kHz and 10 MHz. Cyclic voltammogram (CV) was tested in a three-electrode system, which worked within a scanning speed of 0.2 mV/s between a potential range of 2.5–4.6 V.

Results and discussion

The XRD patterns of prepared pristine NCM-523 and Cerium-doped NCM-523 samples are shown in Fig. 1. All peaks are highly indexed to the α - NaFeO_2 structure (R-3m) [26] and no extra phase peaks of impurities exist. Obvious splitting of the (006)/(102) and (108)/(110) peaks means the formation of layered structure. Cerium doping does not change the basic NCM-523 crystal structure. The lattice parameters of the samples and the values of $I_{(003)}/I_{(104)}$ are shown in Table 1. The values of lattice constant *a* and cell volume *V* increase and become larger as doping amount of Cerium increased, which can be attributed to the larger size of Ce^{4+} than $\text{Co}^{3+}/\text{Mn}^{4+}$. What is more, the (003) peaks of XRD shift to the right with the addition of Ce. The more Ce doped, the more the peaks shifted. Above changes indicate that the doping Ce^{4+} ions might be incorporated into the crystal lattice. As is known, the integrated intensity ratio of $I_{(003)}/I_{(104)}$ is regarded as an important sign to determine the cation mixing degree in the lattice [27]. The values of $I_{(003)}/I_{(104)}$ are 1.45574, 1.45792, 1.46025 and 1.46051 for the pristine and doped samples, respectively. Both ratios are larger than 1.2, which states a highly ordered α - NaFeO_2 structure with limited cation mixing.

Figure 2 shows the SEM data of prepared pristine NCM-523 and Cerium-doped NCM-523 samples. As shown, there is no great difference between them. They both consist of primary particles and secondary particles. The secondary particles exhibit a uniform near spherical

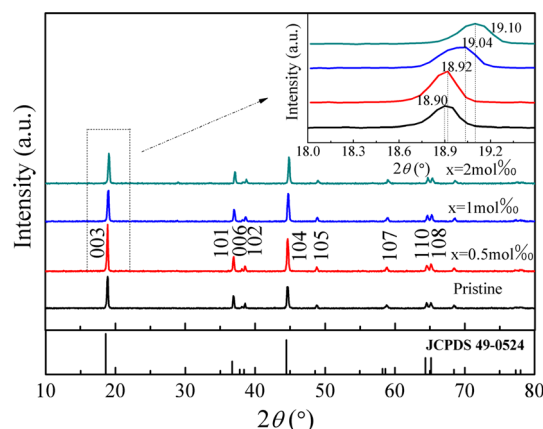
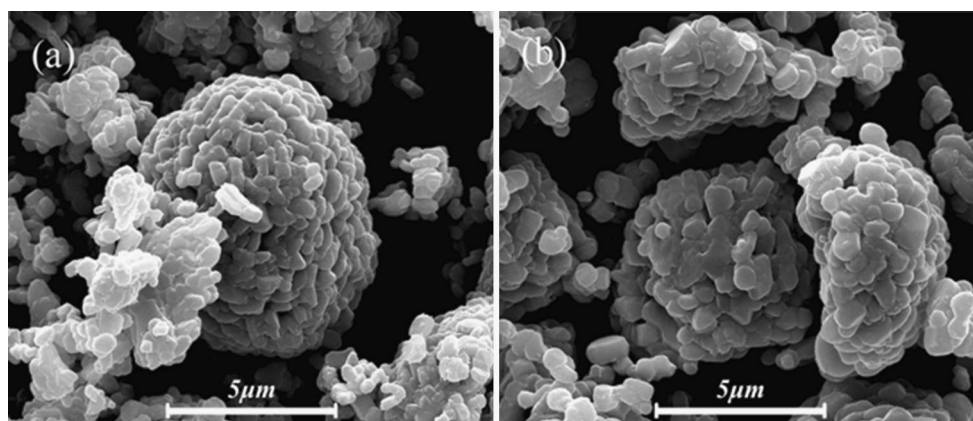


Fig. 1 X-ray diffraction patterns of pristine and Cerium-doped NCM-523 samples

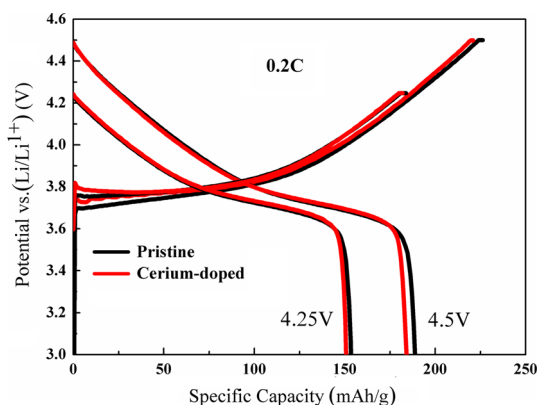
Table 1 Lattice parameters of samples and the values of $I_{(003)}/I_{(104)}$

	Lattice parameters				$I_{(003)}/I_{(104)}$
	a (Å)	c (Å)	V (Å ³)	cla	
Pristine	2.85801	14.17348	100.26	4.95921	1.45574
$x = 0.5$ mol%	2.85902	14.17081	100.29	4.95652	1.45792
$x = 1$ mol%	2.85905	14.17043	100.31	4.95634	1.46025
$x = 2$ mol%	2.85910	14.17167	100.35	4.95668	1.46051

Fig. 2 SEM images of pristine and Cerium-doped NCM-523 samples (**a** pristine, **b** Cerium-doped)

microstructure with a size of 5 μm , which is made up of numerous primary grains. Thus, Cerium doping did not change the morphology of material.

The initial charge–discharge profiles of the pristine and Cerium-doped NCM-523 samples at a rate of 0.2 C in the potential range of 3–4.25 and 3–4.5 V at room temperature are shown in Fig. 3. As shown, all of the stable and smooth curves display a typical electrochemical behavior without an apparent voltage plateau, which indicates that no related phases are formed during charging and discharging. As seen in Fig. 3, the initial discharge capacity of pristine and Cerium-doped samples are 154.59 mAh/g and 150.86 mAh/g at 4.25 V, respectively, with coulomb efficiency of

**Fig. 3** Initial charge–discharge curves of pristine and Cerium-doped NCM-523 samples at different cut-off potentials of 4.25 and 4.5 V

81.97 and 82.92 %, while the corresponding initial discharge capacity at 4.5 V are 188.81 mAh/g and 184.12 mAh/g with coulomb efficiency of 83.41 and 83.29 %. It is seen that the initial discharge capacity of the Cerium-doped sample is lower than that of NCM-523 both at 4.25 and 4.5 V, which should be ascribed to the decrease in the electrochemically active ions [28] in the prepared products doped by a small amount of Cerium. The coulomb efficiency of Cerium-doped NCM-523 is better than that of pristine one. The likely explanation is Cerium doping effectively suppressed the $\text{Li}^+/\text{Ni}^{2+}$ mixing degree so that limited Li^+ is blocked by Ni^{2+} .

Rate capability of the pristine and Cerium-doped NCM-523 samples is shown in Fig. 4. The cells are charged–discharged at different rates of 0.2, 0.5, 1, 2, and 5 C in the potential region of 3–4.25 and 3–4.5 V for every five cycles. It is clear that Cerium-doped NCM-523 exhibits a superior rate capability than the pristine one. From Fig. 4, we can clearly see that although the discharged capacity of pristine sample is higher than that of the Cerium-doped sample at 0.2 C, they all drop off dramatically with increasing C-rates due to polarization [18]. The pristine material displays a higher discharge capacity at low C-rates. However, Cerium-doped one shows better rate capability and capacity retention than the pristine material above 0.5 C. Cerium doping is favorable to improve the rate capacity of NCM-523, especially at high potential of 4.5 V. When charged to 4.5 V, Cerium-doped NCM-523 discharges a capacity of 109.75 mAh/g at 5 C, which is

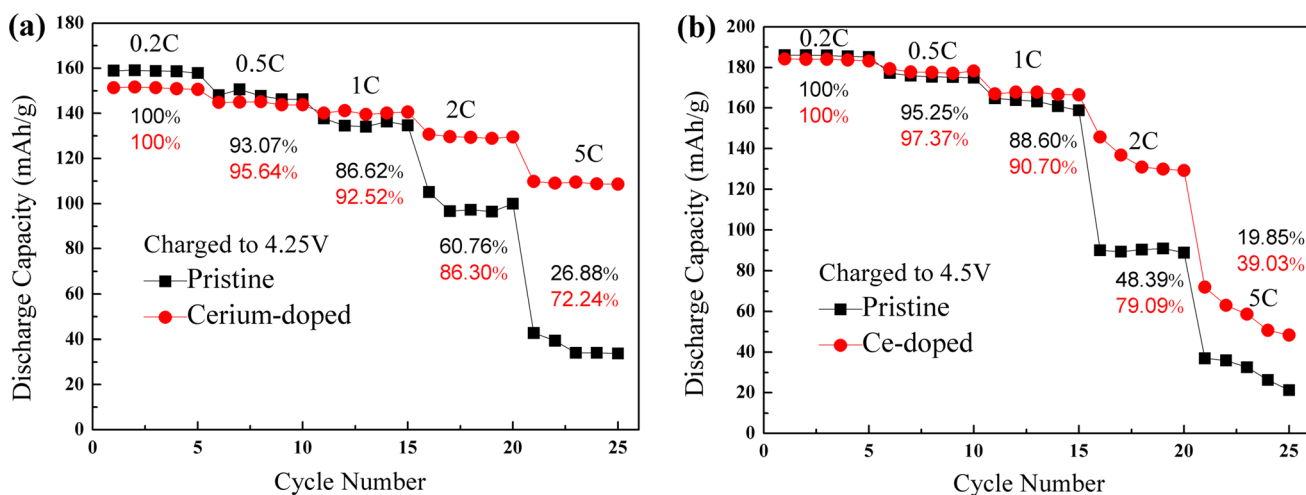


Fig. 4 Rate capability of pristine and Cerium-doped NCM-523 samples at different cut-off potentials of **a** 4.25 V and **b** 4.5 V

2.56 times higher than 42.72 mAh/g of pristine one. When charged to 4.25 V, doped sample presents 71.87 mAh/g at 5 C, which is only 1.94 times higher than 36.92 mAh/g of pristine one. The results reveal that Cerium doped-NCM523 expresses better rate capacity at 4.5 V than at 4.25 V. The increasing stability of the layered crystal structure can be attributed to the doping of inactive Cerium which is more effective especially at high rate and high potential. Namely, Cerium doping is powerful to enhance the capacity at high rate and high potential charge-discharge.

The impact of Cerium doping on the cycling performance of NCM-523 is also investigated in Fig. 5. As seen, although the Cerium-doped material has lower initial discharge capacities, it shows excellent cycle stability and better capacity retention than pristine one at 1 C after 30 cycles. The capacity retention of Cerium-doped NCM-523 is increased to 96.77 % from 93.28 % of pristine sample at

4.25 V and to 97.35 % from 90.90 % at 4.5 V. What is more, the discharge capacity of Cerium-doped material is higher than that of pristine one after cycles. The profiles obviously show that the increased capacity degree for Cerium-doped NCM-523 to pristine sample after 30 cycles at 4.5 V is higher than that at 4.25 V. One possible reason is the stability of inactive ion Cerium. There is no oxidation and reduction during charge-discharge process, so a small amount Cerium doped into layered crystal structure could be a “backbone” role in the layered structure. This “backbone” function works effectively in the cycle process, especially at high potential. What is more, Less Ni²⁺ occupies the sites of Li⁺, which could also enhance the diffuser efficiency of Li⁺ and improve cyclic performance.

The EIS profiles of pristine and Cerium-doped LiNi_{0.5}Co_{0.2}Mn_{0.3}O₂ samples after 10 cycles and 30 cycles are exhibited in Fig. 6. The equivalent circuit is shown in Fig. 6c to further understand the effect of Cerium doping. *R_s* is the solution resistance, corresponding to the small break in the high frequency. *R_{sei}* is the impedance for a solid electrolyte interface layer, related to the arc in the medium frequency region. *R_{ct}* is a charge-transfer at the electrolyte/electrode interface, corresponding to the arc in the low frequency region. *Z_w* is the diffusion of Li ions in the crystal lattice, related to the quasi-straight line in the low frequency [15, 29]. All characteristic parameters were obtained via zview-2soft. The *R_s* values of both samples changed slightly with cycle times increased. The *R_{sei}* values of pristine NCM-523 are almost equal to that of the Cerium-doped sample after 10 or 30 cycles, which indicate that the solid electrolyte interface layer formed on the surface of the electrode has no great distinction. But there is obvious difference between their charge-transfer impedances. The *R_{ct}* values of the pristine LiNi_{0.5}Co_{0.2}Mn_{0.3}O₂ is

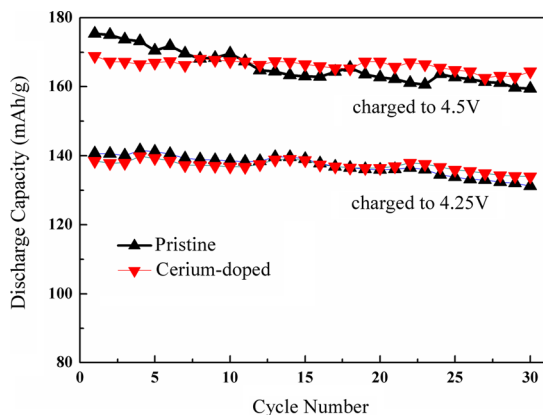


Fig. 5 Cyclic ability of pristine and Cerium-doped NCM-523 samples at different cut-off potentials of 4.25 and 4.5 V

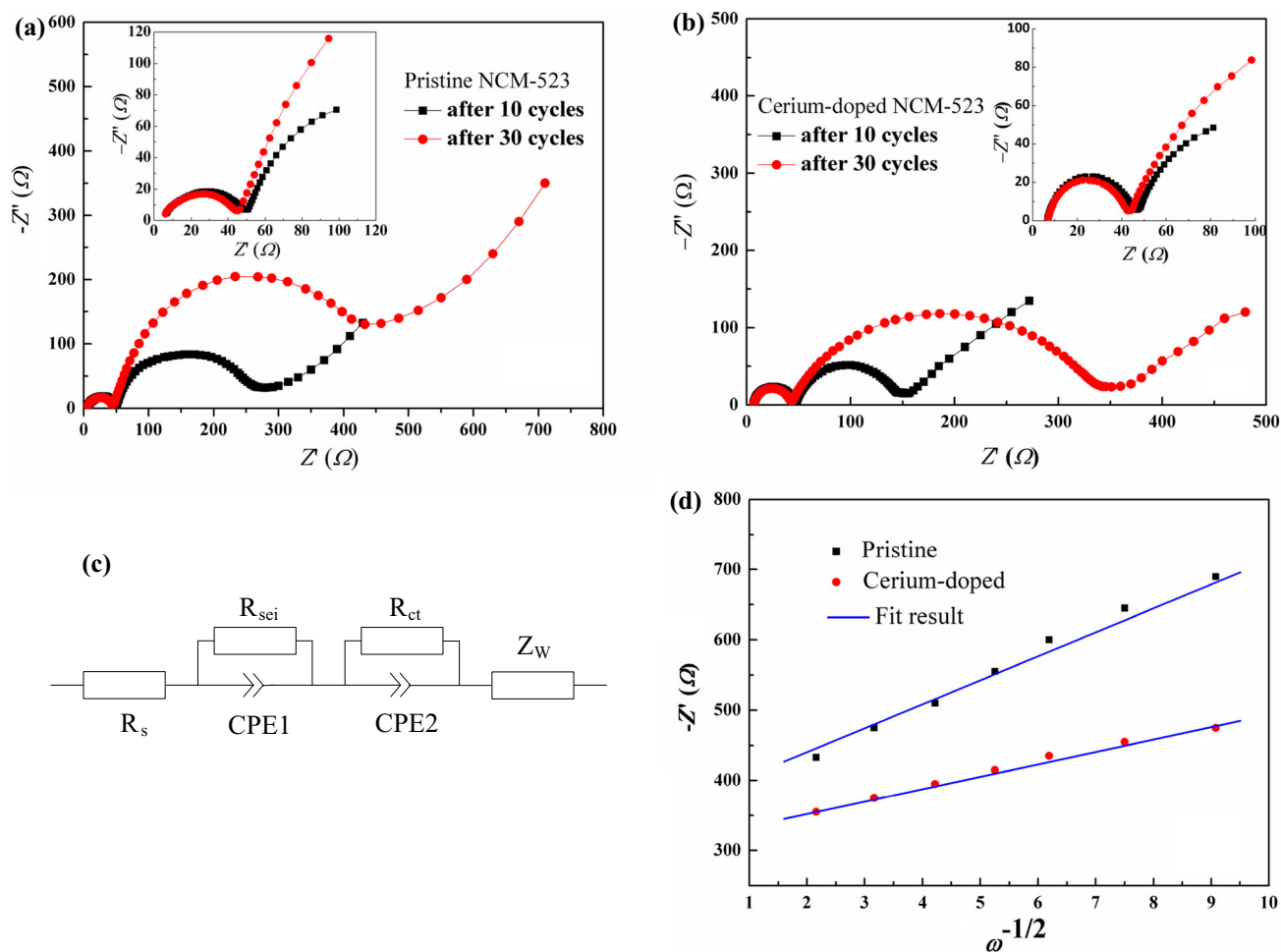


Fig. 6 EIS plots of **a** pristine and **b** Cerium-doped NCM-523 samples after 10th and 30th cycles, **c** equivalent circuit performed to fit the Nyquist plots in **a** and **b** and **d** the relationship plot between inverse square root of angular frequency $\omega^{-1/2}$ and Z'

228.71 Ω after 10 cycles, and then enlarges to 387.7 Ω after 30 cycles. By contrast, the R_{ct} of the Cerium-doped sample only increases from 108.67 Ω after 10 cycles to 308.43 Ω after 30 cycles. The lower R_{ct} of doped material indicates that the Cerium doping may cause some defects in the system, which increases the electronic conductivity and improves the Li^+ kinetic behavior. Therefore, it could be claimed that Cerium doping has a significant function on reducing the increasing of charge-transfer impedance during cycling.

The diffusion coefficient of lithium ions for cells can be calculated according to the following equation: [30]

$$D = 0.5 \times R^2 T^2 / (n A F^2 \sigma C)^2 \quad (1)$$

and [31]

$$Z' = R_s + R_{ct} + \sigma \omega^{-1/2}, \quad (2)$$

where R is the gas constant (8.314 J/(mol K)), T is the absolute temperature (298.15 K), n is the number of electrons per molecule during oxidization, A is the area of

interface between cathode material and electrolyte (here A is 2.00 cm^2), F is the Faraday constant, σ is the Warburg factor, and C is the concentration of lithium ion. From the plot of the relationship between inverse square root of angular frequency $\omega^{-1/2}$ and Z' , σ corresponding to the slop in Fig. 6d can be obtained. So, according to the Eq. (1), Cerium-doped NCM-523 after 30 cycles has a better D_{Li^+} of $1.84 \times 10^{-13} \text{ cm}^2/\text{s}$, compared to $5.47 \times 10^{-14} \text{ cm}^2/\text{s}$ for pristine material. A possible reason is that Li^+ is easier to intercalate/deintercalate with lattice parameters a increased by Cerium doping. Thus, lower charge-transfer impedance and better diffusion coefficient of lithium ions confirm the effect of Cerium-doped layered NCM-523 again, and support the excellent rate capability and cycling stability shown in Figs. 4 and 5.

Cyclic voltammogram curves of pristine and Cerium-doped $\text{LiNi}_{0.5}\text{Co}_{0.2}\text{Mn}_{0.3}\text{O}_2$ cells are exhibited in Fig. 7. As seen, both curves had a similar profile with a couple of redox peaks. The anodic peak for pristine NCM-523 appears at 3.98 V, accompanied with the cathodic peak at

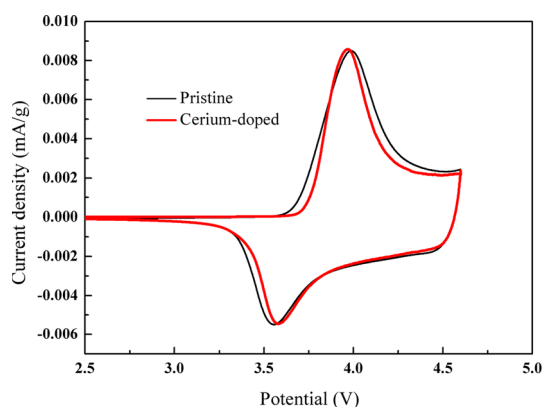


Fig. 7 Cyclic voltammogram curves of pristine and Cerium-doped NCM-523 cells

3.55 V. For doped sample, the anodic peak is observed at 3.96 V, while the corresponding reduction peak shifts up to 3.58 V. It is obvious that the potential difference of redox couple is greatly reduced, when compared with that of pristine sample. Namely, Cerium doping reduces the potential difference between anodic and cathodic peaks. The smaller difference indicates limited electrode polarization and better reversibility of Li ions during electrode reaction, which also means better capacity retention during cycling.

Conclusion

The composition, structure, morphology, and electrochemical performance of pristine and Cerium-doped NCM-523 materials synthesized by co-precipitation and solid-state methods were studied via XRD, SEM, EIS, and CV tests. The electrochemical properties of the pristine and Cerium-doped $\text{LiNi}_{0.5}\text{Co}_{0.2}\text{Mn}_{0.3}\text{O}_2$ cathode materials were compared at conventional potential of 4.25 V and higher potential of 4.5 V. XRD results showed that Cerium did not change the layer structure and might be incorporated into the crystal lattice. Electrochemical test indicated that Cerium-doped samples had outstanding high rate capability and cycling stability, especially at high potential of 4.5 V, when compared to the pristine one. EIS exhibited that Cerium doping contributed to the decreasing of charge-transfer impedance and increasing of diffusion coefficient of lithium ions. Thus, Cerium doping was meaningful to $\text{LiNi}_{0.5}\text{Co}_{0.2}\text{Mn}_{0.3}\text{O}_2$, especially at high potential.

Acknowledgements This work presented herein would not be possible without the Key Scientific and Technological Research and Development Program (Grant no. 2013FZ0065 and no. 2014GZX0006) in Sichuan Province, PR China. We would like to acknowledge them for the financial support.

References

- Li JG, Wang L, Zhang Q, He XG (2009) Synthesis and characterization of $\text{LiNi}_{0.6}\text{Mn}_{0.4-x}\text{Co}_x\text{O}_2$ as cathode materials for Li-ion batteries. *J Power Sources* 189:28–33
- Kim Y (2013) Encapsulation of $\text{LiNi}_{0.5}\text{Co}_{0.2}\text{Mn}_{0.3}\text{O}_2$ with a thin inorganic electrolyte film to reduce gas evolution in the application of lithium ion batteries. *PCCP* 15:6400–6405
- Ramadesigan V, Northrop PWC, De S (2012) Modeling and simulation of lithium-ion batteries from a systems engineering perspective. *J Electrochem Soc* 159:R31–R45
- Fergus JW (2010) Recent developments in cathode materials for lithium ion batteries. *J Power Sources* 195:939–954 [4] J.W. Fergus
- Liu XZ, Li HQ, Li D (2013) PEDOT modified $\text{LiNi}_{1/3}\text{Co}_{1/3}\text{Mn}_{1/3}\text{O}_2$ with enhanced electrochemical performance for lithium ion batteries. *J Power Sources* 243:374–380
- Chen Y, Wang GX, Konstantinov K, Liu HK, Dou SX (2003) Synthesis and characterization of $\text{LiCo}_x\text{Mn}_y\text{Ni}_{1-x-y}\text{O}_2$ as a cathode material for secondary lithium batteries. *J Power Sources* 119:184–188
- Kong JZ, Zhai HF, Ren C (2013) Synthesis and electrochemical performance of macroporous $\text{LiNi}_{0.5}\text{Co}_{0.2}\text{Mn}_{0.3}\text{O}_2$ by a modified sol–gel method. *J Alloys Compd* 577:507–510
- He YB, Ning F, Yang QH (2011) Structural and thermal stabilities of layered $\text{Li}(\text{Ni}_{1/3}\text{Co}_{1/3}\text{Mn}_{1/3})\text{O}_2$ materials in 18650 high power batteries. *J Power Sources* 196:10322–10327
- Kam KC, Doeff MM (2011) Aliovalent titanium substitution in layered mixed Li–Mn–Co oxides for lithium battery applications. *J Mater Chem* 21:9991–9993
- Kitaura H, Hayashi A, Tadanaga K (2010) Electrochemical performance of all-solid-state lithium secondary batteries with Li–Ni–Co–Mn oxide positive electrodes. *Electrochim Acta* 55:8821–8828
- Wu KC, Wang F, Gao LL, Li MR, Xiao LL (2012) Effect of precursor and synthesis temperature on the structural and electrochemical properties of $\text{LiNi}_{0.5}\text{Co}_{0.2}\text{Mn}_{0.3}\text{O}_2$. *Electrochim Acta* 75:393–398
- Yang CC, Lian ZY, Lin SJ (2014) Preparation and application of PVDF-HFP composite polymer electrolytes in $\text{LiNi}_{0.5}\text{Co}_{0.2}\text{Mn}_{0.3}\text{O}_2$ lithium-polymer batteries. *Electrochim Acta* 134:258–265
- Cho YH, Jang D, Yoon J (2013) Thermal stability of charged $\text{LiNi}_{0.5}\text{Co}_{0.2}\text{Mn}_{0.3}\text{O}_2$ cathode for Li-ion batteries investigated by synchrotron based in situ X-ray diffraction. *J Alloys Compd* 562:219–223
- Hou PY, Wang XQ, Song DW (2014) Synthesis, and performances of double-shelled $\text{LiNi}_{0.5}\text{Co}_{0.2}\text{Mn}_{0.3}\text{O}_2$ as cathode for long-life and safe Li-ion battery. *J Power Sources* 265:174–181
- Fey GTK, Muralidharan P, Lu CZ, Cho YD (2006) Enhanced electrochemical performance and thermal stability of La_2O_3 -coated LiCoO_2 . *Electrochim Acta* 51:4850–4858
- Kong JZ, Ren C, Tai GA (2014) Ultrathin ZnO coating for improved electrochemical performance of $\text{LiNi}_{0.5}\text{Co}_{0.2}\text{Mn}_{0.3}\text{O}_2$ cathode material. *J Power Sources* 266:433–439
- Yang K, Fan LZ, Guo J (2012) Significant improvement of electrochemical properties of AlF₃-coated $\text{LiNi}_{0.5}\text{Co}_{0.2}\text{Mn}_{0.3}\text{O}_2$ cathode materials. *Electrochim Acta* 63:363–368
- Liu W, Wang M, Gao XL (2012) Improvement of the high-temperature, high-voltage cycling performance of $\text{LiNi}_{0.5}\text{Co}_{0.2}\text{Mn}_{0.3}\text{O}_2$ cathode with TiO_2 coating. *J Alloys Compd* 543: 181–188
- Huang YH, Chou HL, Wang FM, Hwang BJ (2013) Synergy between experiment and simulation in describing the electrochemical performance of Mg-doped $\text{LiNi}_x\text{Co}_y\text{Mn}_z\text{O}_2$ cathode

- material of lithium ion battery. *Int J Electrochem Sci* 8:8005–8018
20. Woo SW, Myung ST, Bang H, Kim DW, Sun YK (2009) Improvement of electrochemical and thermal properties of $\text{Li}[\text{Ni}_{0.8}\text{Co}_{0.1}\text{Mn}_{0.1}]\text{O}_2$ positive electrode materials by multiple metal (Al, Mg) substitution. *Electrochim Acta* 54:3851–3856
 21. Zhu HL, Xie T, Chen ZY (2014) The impact of vanadium substitution on the structure and electrochemical performance of $\text{LiNi}_{0.5}\text{Co}_{0.2}\text{Mn}_{0.3}\text{O}_2$. *Electrochim Acta* 135:77–85
 22. Sun CS, Zhou Z, Xu ZG, Wang DG, Wei JP, Bian XK, Yan J (2009) Improved high-rate charge/discharge performances of LiFePO_4/C via V-doping. *J Power Sources* 193:841–845
 23. He YS, Pei L, Liao XZ (2007) Synthesis of $\text{LiNi}_{1/3}\text{Co}_{1/3}\text{Mn}_{1/3}\text{O}_{2-z}\text{F}_z$ cathode material from oxalate precursors for lithium ion battery. *J Fluorine Chem* 128:139–143
 24. Wu C, Luo SH, Tian Y, Zhang ZT (2009) Study on electrochemical properties of Ce-doped LiFePO_4 cathode materials. *J Cn Ceramic Soc* 28:153–156
 25. Zhong SK, Wang Y, Liu JQ, Wan K (2011) Synthesis and electrochemical properties of Ce-doped $\text{LiNi}_{1/3}\text{Mn}_{1/3}\text{O}_2$ cathode material for Li-ion batteries. *J Rare Earths* 29:891–895
 26. Ohzuku T, Ueda A (1994) Solid-state redox reactions of LiCoO_2 (R-3m) for 4 volt secondary lithium cells. *J Electrochem Soc* 141:2972–2977
 27. Myung ST, Izumi K, Komaba S, Yashiro H (2007) Functionality of oxide coating for $\text{Li}[\text{Li}_{0.05}\text{Ni}_{0.4}\text{Co}_{0.15}\text{Mn}_{0.4}]\text{O}_2$ as positive electrode materials for lithium-ion secondary batteries. *J Phys Chem C* 111:4061–4067
 28. Wang M, Chen YB, Wu F, Su YF, Chen L (2010) Characterization of yttrium substituted $\text{LiNi}_{0.33}\text{Mn}_{0.33}\text{Co}_{0.33}\text{O}_2$ cathode material for lithium secondary cells. *Electrochim Acta* 55:8815–8820
 29. Zhang ZR, Liu HS (2004) Electrochemical performance and spectroscopic characterization of TiO_2 -coated $\text{LiNi}_{0.8}\text{Co}_{0.2}\text{O}_2$ cathode materials. *J Power Sources* 129:101–106
 30. Li Z, Du F, Bie XF (2010) Electrochemical kinetics of the $\text{Li}[\text{Li}_{0.23}\text{Co}_{0.3}\text{Mn}_{0.47}]\text{O}_2$ cathode material studied by GITT and EIS. *J Phys Chem C* 114:22751–22757
 31. Ni J, Zhou H, Chen J, Zhang X (2008) Improved electrochemical performance of layered $\text{LiNi}_{0.4}\text{Co}_{0.2}\text{Mn}_{0.4}\text{O}_2$ via Li_2ZrO_3 coating. *Electrochim Acta* 53:3075–3308